# CHEMISTRY
## A European Journal

## Supporting Information

# Synthesis and Analysis of the Conformational Preferences of 5-Aminomethyloxazolidine-2,4-dione Scaffolds: First Examples of β²- and β²,²-Homo-Freidinger Lactam Analogues

Arianna Greco, Sara Tani, Rossella De Marco,* and Luca Gentilucci*[a]
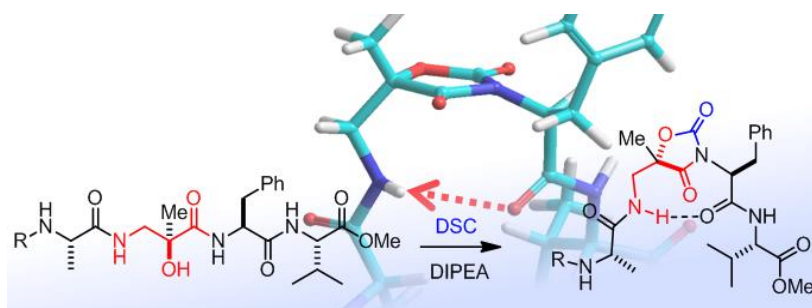
chem_201402519_sm_miscellaneous_information.pdf

### Table of contents

*Plausible reaction pathway for the synthesis of Amo-peptides.*

A plausible reaction pathway for the cyclization of the model peptide Ts-Ala-*iso*Ser-PheNH$_2$ to Ts-Ala-Amo-PheNH$_2$ with DSC and catalytic DIPEA is depicted in Scheme S1. In the proposed mechanism, the cyclization to Amo proceeds *via* the *iso*Ser-*O*-succinimidyl carbonate intermediate **A**. The intermediate **A** is deprotonated by DIPEA at PheNH, giving the 5-membered anionic intermediate **B** with endocyclic C=O (path **a**). The loss of 2,5-dioxopyrrolidin-1-olate leaving group, rapidly protonated by DIPEAH$^+$, leads to the Amo-peptide **3** and DIPEA, which can be utilized in catalytic amount. The intermediate **A** can be deprotonated at *iso*SerNH as well (path **b**); this could give access to the alternative 5-membered cyclic anionic intermediate **C** with hexocyclic C=O, precursor of a Oxd-peptide.

Preliminary computations were performed for the intermediates **B** and **C** employing Density Functional Theory; a systematic conformational analysis for the structures was done at the B3LYP/6-311++G(d,p) level. Optimization was performed by conjugate gradient algorithm, convergence at 0.001. The results indicate that the intermediate **B** is about 2.0 Kcal mol$^{-1}$ more stable than the alternative intermediate **C**.
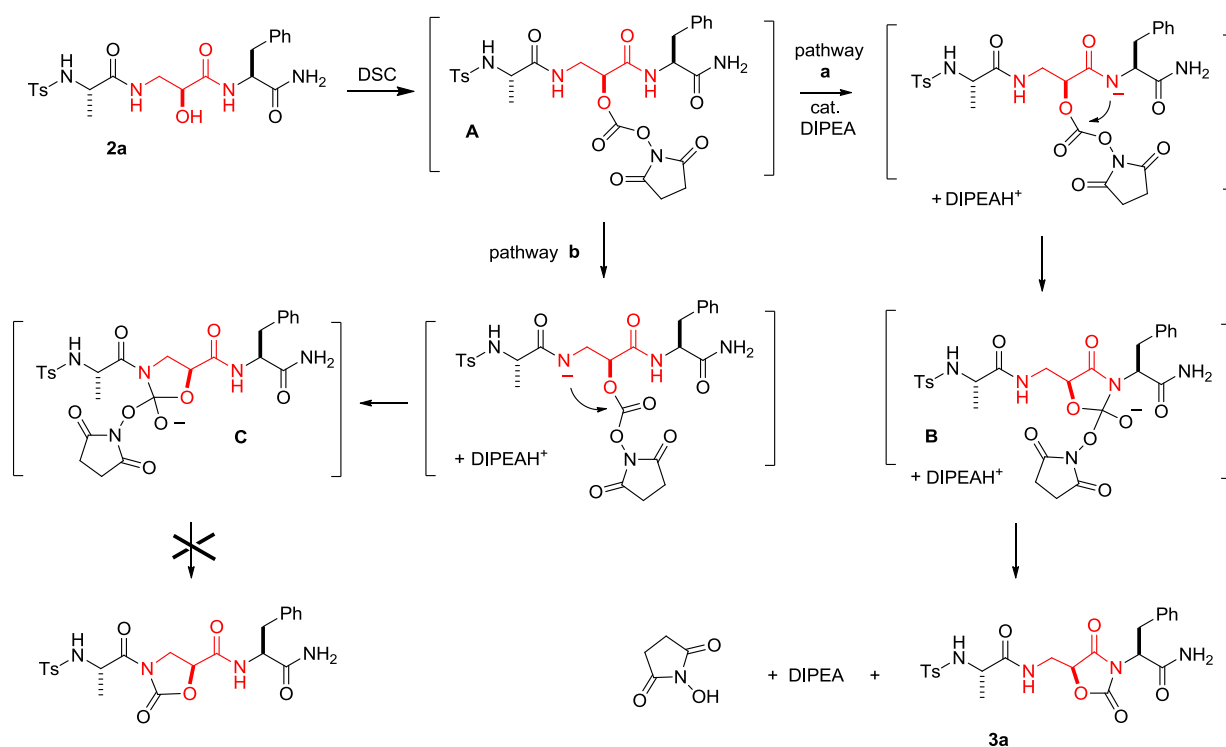


Scheme S1. Cyclization of the model peptide Ts-Ala-*iso*Ser-PheNH$_2$ **2** to Ts-Ala-Amo-PheNH$_2$ **3**.

Table S1. Δδ/Δt values (p.p.b./°K) for the amide protons of peptides **3a**, **3b**, **3c**, **3f**, **5**, in CDCl$_3$.

| Compd | sequence | AlaNH | AmoNH | ValNH | CONH$_2$ |
|-------|----------|-------|-------|-------|----------|
| **3a** | Ts-Ala-(S)-Amo-PheNH$_2$ | -15.1 | -8.1 | - | -14.3/-9.7 |
| **3b** | Ts-Ala-(R)-Amo-PheNH$_2$ | -8.6 | -6.2 | - | -8.6/-8.0 |
| **3c** | Ts-Ala-(S)-Amo-(R)-PheNH$_2$ | -8.4 | -6.0 | - | -7.7/-9.5 |
| **3f** | Boc-Ala-(S)-Amo-Phe-ValOMe | -4.5 | -5.0 | -4.5 | - |
| **5** | Ts-Ala-(R)-5-hydroxyAmo-PheNH$_2$ | -14.7 | -10.0 | - | -13.7/-11.0 |

*Circular dichroism of **3d**, **3d**, **10a**, and **10b** recorded in DCM.*

ECD spectra were recorded from 200 to 400 nm at 25 °C. 1 mM solutions were made up in spectral grade solvents and run in a 0.1 cm quartz cell (Figure S1). Data are reported in molar ellipticity [θ] (deg cm$^2$ dmol$^{-1}$).
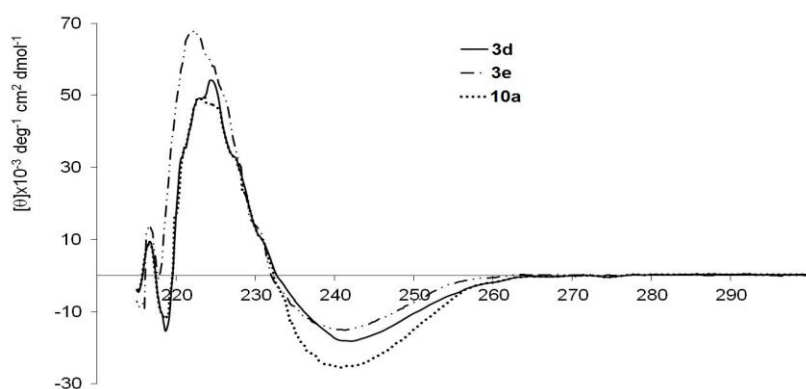


Figure S1. ECD spectra of **3d**, **3e**, **10a**, and **10b** recorded in DCM at r.t.; **3d** and **10b** are practically superimposed.

*IR analyses **3d**, **3e**, **10a**, and **10b** in DCM.*

The compounds were dried in vacuo, and all the sample preparations were performed under nitrogen atmosphere. All infrared spectra were obtained for 1 mM solutions in dry DCM at 297 °K at 2 cm$^{-1}$ resolution, using a 1 mm NaCl solution cell and a FT-IR spectrometer (64 scans). (Figure S2).



Figure S2. Amide NH stretching regions of the IR absorption spectra for samples of 2 mM **3d**, **3e**, **10a**, and **10b** in DCM at r.t.

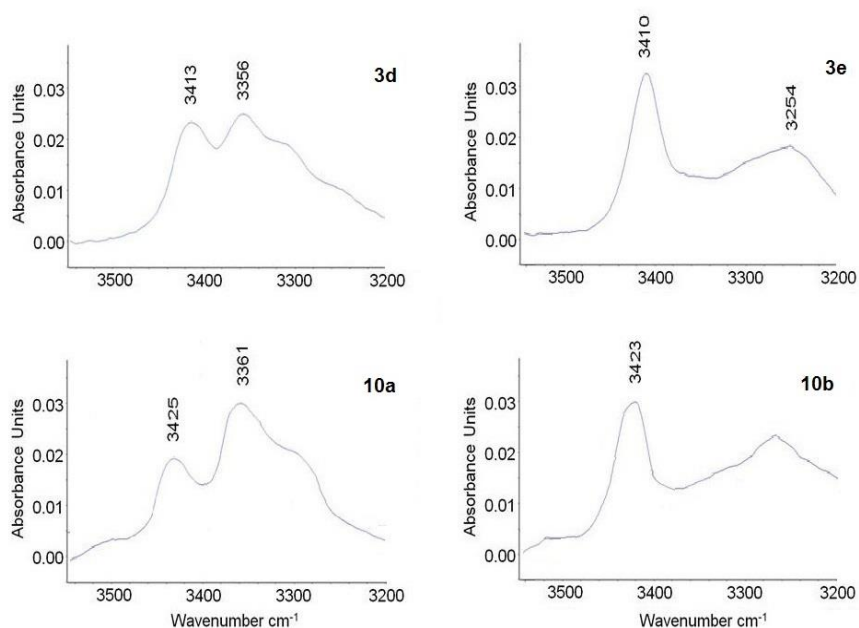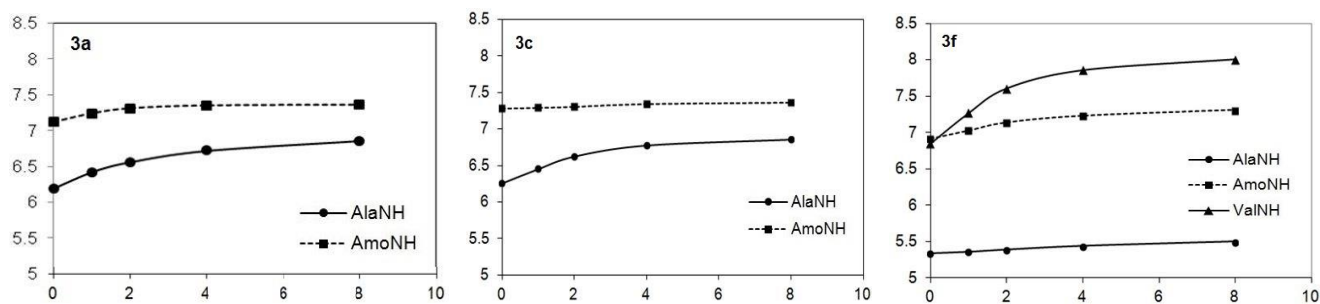Figure S3. Titration experiments: variation of NH proton chemical shift (p.p.m.) of 2 mM **3a**, **3c**, **3f**, in CDCl$_3$ as a function of increasing [D$_6$]DMSO (from 0 to 8 % v/v).

Table S2. Non-obvious ROESY cross-peaks observed for **3d** in 8:2 [D$_6$]DMSO/H$_2$O.[a]

| Cross-peak | intensity | Cross-peak | Intensity |
|---|---|---|---|
| ValNH-ValMe | vs | PheArH$_{3,5}$-AmoHβ$_{up}$ | m |
| ValNH-AlaMe | w | PheArH$_{3,5}$-PheHβ$_{up}$ | m |
| ValNH-ValHβ | s | PheArH$_{3,5}$-PheHβ$_{dw}$ | w |
| ValNH-TsMe | w | PheArH$_{3,5}$-ValHα | w |
| ValNH-AmoHβ$_{up}$ | w | PheArH$_{3,5}$-PheHα | m |
| ValNH-PheHβ$_{up}$ | w | PheArH$_4$-ValMe | w |
| ValNH-PheHβ$_{dw}$ | s | PheArH$_4$-TsMe | w |
| ValNH-COOMe | w | PheArH$_{2,6}$-ValMe | w |
| ValNH-ValHα | m | PheArH$_{2,6}$-AlaMe | w |
| ValNH-PheHα | vs | PheArH$_{2,6}$-TsMe | w |
| ValNH-AlaNH | w | PheArH$_{2,6}$-AmoHβ$_{up}$ | m |
| ValNH-AmoNH | w | PheArH$_{2,6}$-PheHβ$_{up}$ | vs |
| AmoNH-ValMe | w | PheArH$_{2,6}$-PheHβ$_{dw}$ | s |
| AmoNH-AlaMe | m | PheArH$_{2,6}$-PheHα | vs |
| AmoNH-AmoHβ$_{up}$ | s | AmoHα-AlaMe | m |
| AmoNH-AmoHβ$_{dw}$ | m | AmoHα-AmoHβ$_{up}$ | m |
| AmoNH-AlaHα | vs | AmoHα-AmoHβ$_{dw}$ | vs |
| AmoNH-AmoHα | m | PheHα-ValMe | w |
| AmoNH-TsArH$_{2,6}$ | m | PheHα-ValHβ | w |
| AmoNH-AlaNH | m | PheHα-TsMe | w |
| AlaNH-ValMe | w | PheHα-PheHβ$_{up}$ | m |
| AlaNH-AlaMe | vs | PheHα-PheHβ$_{dw}$ | s |
| AlaNH-PheHβ$_{dw}$ | w | PheHα-COOMe | w |
| AlaNH-AlaHα | m | PheHα-ValHα | w |
| AlaNH-PheHα | w | ValHα-AlaMe | w |
| AlaNH-TsArH$_{2,4}$ | w | ValHα-ValHβ | vs |
| TsArH$_{2,6}$-ValMe | w | ValHα-TsMe | w |
| TsArH$_{2,6}$-AlaMe | s | ValHα-PheHβ$_{up}$ | w |

| Cross-peak | Intensity | Cross-peak | Intensity |
|---|---|---|---|
| TsArH$_{2,6}$-AmoHβ$_{up}$ | w | ValHα-PheHβ$_{dw}$ | w |
| TsArH$_{2,6}$-AmoHβ$_{dw}$ | m | COOMe-ValHβ | m |
| TsArH$_{2,6}$-AlaHα | s | PheHβ$_{dw}$-AlaMe | w |
| TsArH$_{2,6}$-ValHα | w | PheHβ$_{up}$-ValMe | m |
| TsArH$_{2,6}$-AmoHα | w | PheHβ$_{up}$-ValHβ | w |
| TsArH$_{3,5}$-ValMe | w | AmoHβ$_{dw}$-AlaMe | w |
| TsArH$_{3,5}$-AlaMe | w | TsMe-ValMe | w |
| TsArH$_{3,5}$-AmoHβ$_{dw}$ | w | TsMe-AlaMe | w |
| TsArH$_{3,5}$-Val Hα | w | TsMe-ValHβ | w |
| TsArH$_{3,5}$-Amo Hα | w | ValHβ-AlaMe | w |
| PheArH$_{3,5}$-AlaMe | w | ValMe-AlaMe | w |

[a] Stereochemistry has been omitted; [b] up = upfield, dw = downfield; [c] vs = very strong,  s = strong, m = medium, w = weak.

Table S3. Non-obvious ROESY cross-peaks observed for **3e** in 8:2 [D$_6$]DMSO/H$_2$O.[a]

| Cross-peak | Intensity | Cross-peak | Intensity |
|---|---|---|---|
| ValNH-ValMe | vs | PheArH$_{3,5}$-PheHβ$_{up}$ | w |
| ValNH-ValHβ | s | PheArH$_{3,5}$-PheHβ$_{dw}$ | w |
| ValNH-AmoHα | w | PheArH$_{3,5}$-Phe Hα | w |
| ValNH-PheHβ$_{up}$ | m | PheArH$_{2,6}$-AlaMe | w |
| ValNH-PheHβ$_{dw}$ | w | PheArH$_{2,6}$-AmoHβ$_{dw}$ | m |
| ValNH-COOMe | w | PheArH$_{2,6}$-PheHβ$_{up}$ | s |
| ValNH-ValHα | m | PheArH$_{2,6}$-PheHβ$_{dw}$ | vs |
| ValNH-PheHα | vs | PheArH$_{2,6}$-PheHα | vs |
| ValNH-AlaNH | w | AmoHα-ValMe | w |
| ValNH-AmoNH | w | AmoHα-AmoHβ$_{up}$ | m |
| AmoNH-ValMe | w | AmoHα-AmoHβ$_{dw}$ | m |
| AmoNH-AlaMe | m | AmoHα-PheHβ$_{dw}$ | w |
| AmoNH-AmoHβ$_{up}$ | m | AmoHα-ValHα | w |
| AmoNH-AmoHβ$_{dw}$ | s | PheHα-ValMe | w |
| AmoNH-AlaHα | vs | PheHα-ValHβ | w |
| AmoNH-AmoHα | w | PheHα-PheHβ$_{up}$ | s |
| AmoNH-AlaNH | w | PheHα-PheHβ$_{dw}$ | m |
| AlaNH-ValMe | w | PheHα-ValHα | w |
| AlaNH-AlaMe | vs | ValHα-AlaMe | m |
| AlaNH-AmoHα | w | ValHα-ValHβ | m |
| AlaNH-AlaHα | s | ValHα-ValMe | vs |

| Cross-peak | intensity | Cross-peak | Intensity |
|---|---|---|---|
| AlaNH-TsArH$_{2,6}$ | s | ValHα-AmoHβ$_{dw}$ | w |
| AlaNH-TsArH$_{3,5}$ | s | ValHα-PheHβ$_{up}$ | w |
| TsArH$_{2,6}$-ValMe | w | ValHα-PheHβ$_{dw}$ | w |
| TsArH$_{2,6}$-AlaMe | m | COOMe-ValMe | w |
| TsArH$_{2,6}$-AlaHα | m | COOMe-ValHβ | w |
| TsArH$_{2,6}$-ValHα | w | COOMe-PheHβ$_{up}$ | s |
| TsArH$_{2,6}$-AmoHα | w | AlaHα-TsMe | w |
| TsArH$_{2,6}$-PheHα | w | TsMe-AlaMe | w |
| TsArH$_{3,5}$-ValMe | w | TsMe-ValHβ | m |
| TsArH$_{3,5}$-AlaMe | w | ValHβ-AlaMe | w |
| PheArH$_{3,5}$-AmoHβ$_{dw}$ | w | ValMe-AlaMe | w |

<sup>a</sup> Stereochemistry has been omitted; <sup>b</sup> up = upfield, dw = downfield; <sup>c</sup> vs = very strong, s = strong, m = medium, w = weak.

Table S4. Non-obvious ROESY cross-peaks observed for **10a** in 8:2 [D$_6$]DMSO/H$_2$O.<sup>a</sup>

| Cross-peak | intensity | Cross-peak | Intensity |
|---|---|---|---|
| ValNH-ValMe | vs | PheArH$_{3,5}$-AlaMe | w |
| ValNH-AlaMe | m | PheArH$_{3,5}$-AmoHβ$_{up}$ | m |
| ValNH-ValHβ | s | PheArH$_{3,5}$-PheHβ$_{up}$ | m |
| ValNH-TsMe | w | PheArH$_{3,5}$-PheHβ$_{dw}$ | w |
| ValNH-AmoHβ$_{up}$ | w | PheArH$_{3,5}$-ValHα | w |
| ValNH-PheHβ$_{up}$ | w | PheArH$_{3,5}$-PheHα | m |
| ValNH-PheHβ$_{dw}$ | s | PheArH$_4$-ValMe | w |
| ValNH-COOMe | w | PheArH$_4$-TsMe | w |
| ValNH-ValHα | m | PheArH$_{2,6}$-ValMe | w |
| ValNH-PheHα | vs | PheArH$_{2,6}$-AlaMe | w |
| ValNH-AlaNH | w | PheArH$_{2,6}$-TsMe | w |
| ValNH-AmoNH | w | PheArH$_{2,6}$-AmoHβ$_{up}$ | m |
| AmoNH-ValMe | w | PheArH$_{2,6}$-PheHβ$_{up}$ | vs |
| AmoNH-AlaMe | m | PheArH$_{2,6}$-PheHβ$_{dw}$ | s |
| AmoNH-AmoMe | m | PheArH$_{2,6}$-PheHα | vs |
| AmoNH-ValHβ | m | PheHα-ValMe | w |
| AmoNH-AmoHβ$_{up}$ | s | PheHα-ValHβ | w |
| AmoNH-AmoHβ$_{dw}$ | m | PheHα-TsMe | w |
| AmoNH-AlaHα | vs | PheHα-PheHβ$_{up}$ | m |
| AmoNH-ValHα | m | PheHα-PheHβ$_{dw}$ | s |
| AmoNH-PheHα | m | PheHα-COOMe | w |
| AmoNH-TsArH$_{2,6}$ | m | PheHα-ValHα | w |
| AmoNH-AlaNH | m | ValHα-AlaMe | m |

| | | | |
|---|---|---|---|
| AlaNH-ValMe | m | ValHα-ValHβ | vs |
| AlaNH-AlaMe | vs | ValHα-TsMe | w |
| AlaNH-ValHβ | w | ValHα-PheHβ$_{up}$ | w |
| AlaNH-PheHβ$_{dw}$ | w | ValHα-AlaHα | m |
| AlaNH-AlaHα | m | ValHα-COOMe | m |
| AlaNH-ValHα | m | ValHα-PheHβ$_{dw}$ | w |
| AlaNH-PheHα | w | COOMe-ValHβ | m |
| AlaNH-TsArH$_{2,4}$ | w | PheHβ$_{dw}$-AlaMe | w |
| TsArH$_{2,6}$-ValMe | w | PheHβ$_{up}$-ValMe | m |
| TsArH$_{2,6}$-AlaMe | s | PheHβ$_{up}$-ValHβ | w |
| TsArH$_{2,6}$-AmoMe | w | AmoHβ$_{dw}$-AlaMe | w |
| TsArH$_{2,6}$-AmoHβ$_{up}$ | w | TsMe-ValMe | w |
| TsArH$_{2,6}$-AmoHβ$_{dw}$ | m | TsMe-AlaMe | w |
| TsArH$_{2,6}$-AlaHα | s | TsMe-ValHβ | w |
| TsArH$_{2,6}$-ValHα | w | ValHβ-AlaMe | m |
| TsArH$_{3,5}$-ValMe | w | AmoMe-AlaMe | w |
| TsArH$_{3,5}$-AlaMe | w | AmoMe-AmoHβ$_{up}$ | m |
| TsArH$_{3,5}$-AmoMe | w | AmoMe-AmoHβ$_{dw}$ | vs |
| TsArH$_{3,5}$-AmoHβ$_{dw}$ | w | AlaMe-ValMe | m |
| TsArH$_{3,5}$-ValHα | w | | |

[a] Stereochemistry has been omitted; [b] up = upfield, dw = downfield; [c] vs = very strong, s = strong, m = medium, w = weak.

Table S5. Non-obvious ROESY cross-peaks observed for **10b** in 8:2 [D$_6$]DMSO/H$_2$O.[a]

| Cross-peak | Intensity | Cross-peak | Intensity |
|---|---|---|---|
| ValNH-ValMe | vs | PheArH$_{3,5}$-PheHβ$_{up}$ | w |
| ValNH-AmoMe | m | PheArH$_{3,5}$-PheHβ$_{dw}$ | w |
| ValNH-ValHβ | s | PheArH$_{3,5}$-PheHα | w |
| ValNH-PheHβ$_{up}$ | m | PheArH$_{2,6}$-AlaMe | w |
| ValNH-PheHβ$_{dw}$ | w | PheArH$_{2,6}$-AmoHβ$_{dw}$ | m |
| ValNH-COOMe | w | PheArH$_{2,6}$-PheHβ$_{up}$ | s |
| ValNH-ValHα | m | PheArH$_{2,6}$-PheHβ$_{dw}$ | vs |
| ValNH-PheHα | vs | PheArH$_{2,6}$-PheHα | vs |
| ValNH-AlaNH | w | PheHα-ValMe | w |
| ValNH-AmoNH | w | PheHα-ValHβ | w |
| AmoNH-ValMe | w | PheHα-PheHβ$_{up}$ | s |
| AmoNH-AlaMe | m | PheHα-PheHβ$_{dw}$ | m |
| AmoNH-AmoMe | m | PheHα-ValHα | w |

| | | | |
|---|---|---|---|
| AmoNH-AmoHβ$_{up}$ | m | ValHα-AlaMe | m |
| AmoNH-AmoHβ$_{dw}$ | s | ValHα-ValHβ | m |
| AmoNH-AlaHα | vs | ValHα-ValMe | vs |
| AmoNH-AlaNH | w | ValHα-AmoHβ$_{dw}$ | w |
| AlaNH-ValMe | w | ValHα-PheHβ$_{up}$ | w |
| AlaNH-AlaMe | vs | ValHα-PheHβ$_{dw}$ | w |
| AlaNH-AmoMe | w | COOMe-ValMe | w |
| AlaNH-AlaHα | s | COOMe-ValHβ | w |
| AlaNH-TsArH$_{2,6}$ | s | COOMe-PheHβ$_{up}$ | s |
| AlaNH-TsArH$_{3,5}$ | s | AlaHα-TsMe | w |
| TsArH$_{2,6}$-ValMe | w | TsMe-AlaMe | w |
| TsArH$_{2,6}$-AlaMe | m | TsMe-ValHβ | m |
| TsArH$_{2,6}$-AmoMe | w | ValHβ-AlaMe | w |
| TsArH$_{2,6}$-AlaHα | m | AmoMe-ValMe | m |
| TsArH$_{2,6}$-ValHα | w | AmoMe-AmoHβ$_{up}$ | m |
| TsArH$_{2,6}$-PheHα | w | AmoMe-AmoHβ$_{dw}$ | m |
| TsArH$_{3,5}$-ValMe | w | AmoMe-PheHβ$_{dw}$ | w |
| TsArH$_{3,5}$-AlaMe | w | AmoMe-ValHα | m |
| PheArH$_{3,5}$-AmoHβ$_{dw}$ | w | AlaMe-ValMe | m |

[a] Stereochemistry has been omitted; [b] up = upfield, dw = downfield; [c] vs = very strong, s = strong, m = medium, w = weak.
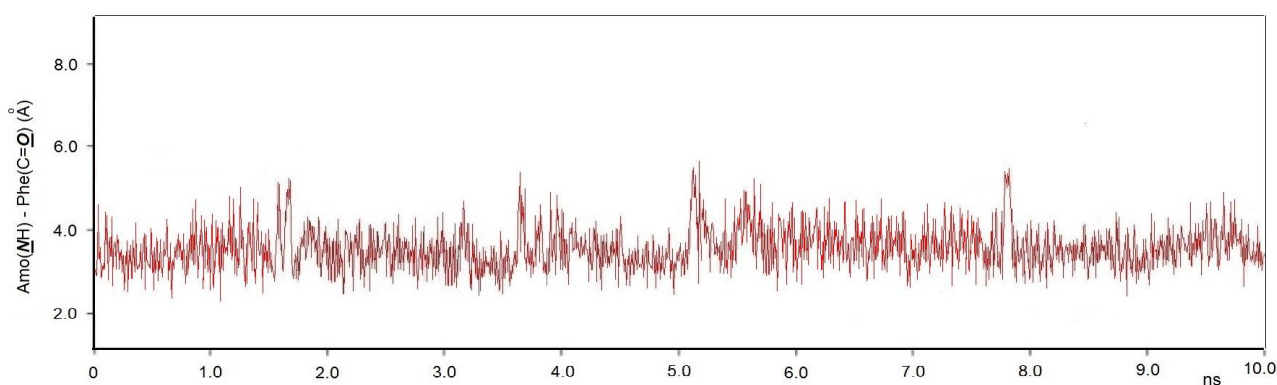


Figure S4. Distances (Å) between the amide nitrogen of Amo[2] and the carbonyl oxygen of Phe[3] sampled from a 10 ns unrestrained Molecular Dynamics simulation of **10a** calculated in a 30x30x30 Å box of equilibrated standard TIP3P water molecules, using the ROESY-derived geometry as starting structure.
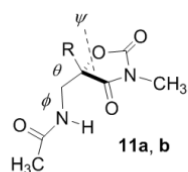
Figure 3. Minimum-energy conformations and relative energies of the *+g*, *trans*, and *-g* rotamers around the central backbone dihedral angle $\theta$ of model compounds **11a** and **11b**. A systematic conformational analysis around $\phi$ and $\theta$ was performed in gas-phase employing DFT; $\Delta E$ are given in kcal/mol; $\phi$, $\theta$, and $\psi$, are given into brackets in degrees; Amo is rendered in balls and cylinders, the rest in sticks.
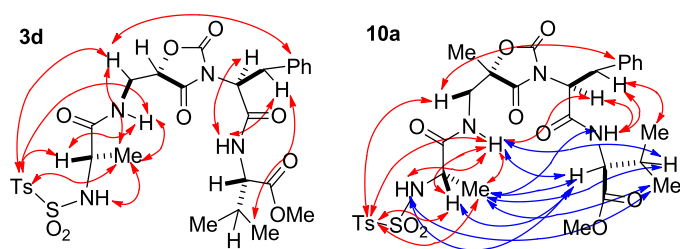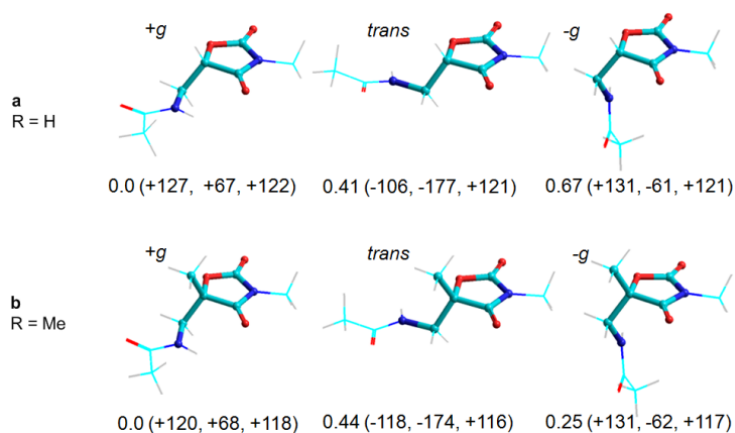


Figure 5. Sketches of the structures of **3d** and **10a**, and short-range (distances ≤ 3 Å) proton-proton ROESY correlations, indicated by arrows. Intra-residue and long-range (> 3 Å) correlations are not shown. Red arrows connect protons belonging to consecutive residues (*i-i+1*), while blue arrows connect protons of non-consecutive residues (*i-i+2* or *i-i+3*).
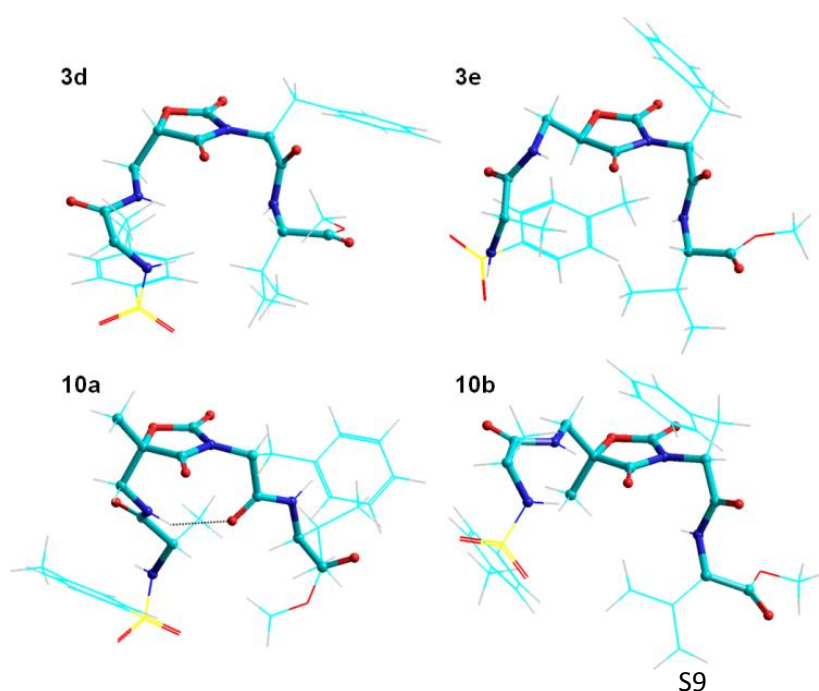


Figure 6. Top, representative lowest energy structures **3d**, **3e**, **10a**, and **10b**, calculated by restrained MD in a 30x30x30 Å box of standard TIP3P water molecules. Backbones and Amo rings are rendered in balls and cylinders, the rest in sticks.

**3a**

**3b**

S11

**3c**

**3d**

3e

**3f**

3g

S20